This is a repository copy of *Annular impinging jet with recirculation zone expanded by acoustic excitation*.

White Rose Research Online URL for this paper:
http://eprints.whiterose.ac.uk/508/

Article:

Annular impinging jet with recirculation zone expanded by acoustic excitation

Zdeněk Trávníček[a] and Václav Tesař[b,]

[a] Institute of Thermomechanics, Czech Academy of Sciences, Dolejškova 5, 182 00, Prague 8, Czech Republic
[b] The University of Sheffield, Mappin Street, Sheffield S1 3JD, UK

Abstract

Flow visualization and mass transfer (naphthalene sublimation) experiments were performed on acoustically excited annular air jet with diameter ratio D_i/D_o=0.95. Two different regimes of the time-mean flow field were found, differing in the size of the central recirculation zone, with either the single stagnation point or the stagnation circle. The switching between the two regimes is accomplished by acoustic excitation, under identical geometry conditions. An effective stabilization of the large recirculation zone, as well as remarkable augmentation of average heat/mass transfer by 23%, have been achieved at the excitation Strouhal number Sh=0.94.

acoAJ	acoustically excited annular jet
AJ	annular jet
B	slot width of the annular nozzle, $(D_o-D_i)/2$
D_i	inner diameter of annular nozzle, D_i=38 mm
D_o	outer diameter of annular nozzle, D_o=40 mm
D_{naph}	mass diffusion coefficient of naphthalene vapor in air, m^2/s
F	frequency, Hz
H	local heat transfer coefficient, W/(m^2 K)
h_m	local mass transfer coefficient, Eq. ([3]), m/s
H	nozzle-to-wall spacing, (see Fig. 1)
K	thermal conductivity, W/(m K)

Nu	local Nusselt number, hD_o/k
Pr	Prandtl number
R	radial coordinate, (see Fig. 1)
Re	Reynolds number of annular jet, defined from the annular nozzle diameter as U_jD_o/ν
Re_B	Reynolds number of annular slot jet, defined from the annular nozzle width as U_jB/ν
Sc	Schmidt number for naphthalene in air, ν/D_{naph}
Sw	local Sherwood number, h_mD_o/D_{naph}
$\overline{Sw}$	average Sherwood number, Eq. (5)
SPL	sound pressure level, dB
SyJ	zero-net-mass-flux synthetic jet
Sh	Strouhal number of annular jet, defined from the annular nozzle diameter as fD_o/U_j
Sh_B	Strouhal number of annular slot jet, defined from the annular nozzle width as fB/U_j
T	temperature, K
Uj	average velocity of the jet from the annular nozzle of diameters D_i, D_o, m/s
x	axial coordinate (see Fig. 1)
y, z	Cartesian coordinates on the exposed wall, (see Fig. 6)
Δt	run time duration of the naphthalene sublimation
Δx	sublimation depth of naphthalene
ν	kinematic viscosity of air

1. Introduction

Impinging jets are the technique for achieving the highest heat and mass transfer performance between a fluid and an exposed wall. They have been studied quite extensively. The most important results are collected in monographs, such as e.g., the outstanding book by Dyban and Mazur [1], and the distinguished work by Martin [2]. Several comprehensive reviews have appeared, particularly relevant being Ref. [3, 4, 5, 6, 7 and 8]. Theoretical, experimental and numerical research of the topic has been continuing up to the present time—as presented e.g., in the recent review by Garimella [8] and recent studies [9, 10, 11, 12, 13, 14, 15 and 16]. The references cited here were chosen to illustrate the wide scope of related investigations; exhaustive collections of literature dealing with the subject are available elsewhere— e.g., [8], apart from discussing his own results, lists 122 relevant references.

The most important area of applications of impinging submerged jets, using gas (usually air) as the working fluid, are cooling, heating and drying. Typical advantages of the impinging submerged jets as well as their 19 main applications were recently summarized by Trávníček et al. [16]. Steady turbulent impinging jets can achieve very high heat/mass transfer rate—the term "steady" meant in the time-mean-flow sense. In fact, the processes in turbulent impinging jet flows are significantly influenced by inherent oscillations and large vortex structures—as described e.g., by Crow and Champagne [17], Hussain [18], and Kataoka et al. [19]. Despite this fact, a possibility to intensify transport process to obtain even higher performance by excitation remains a great challenge for researchers. There are many possibilities which may be roughly divided into the passive and active flow control methods—see e.g., [20]. The passive methods (sometimes called flow management rather than flow control— [21]) require no auxiliary power; they are based on expedient modification of the geometry. The active flow control requires applying external energy. It can be either predetermined (without regard to the particular state of the flow—this method is used in this paper) or reactive (operating with a control loop, which may be either an open feedforward one, or a closed, feedback loop), [20].

Active control of impinging jets can be based either on steady input action or on applied oscillation. The former case was investigated e.g., by Hwang et al. [22]: heat transfer of an axisymmetric impinging jet was enhanced by means of a steady co-flowing or counter flowing control jet. Another recent approach by Trávníček et al. [16] uses the existence of two stable states of an annular impinging jet with Coanda-effect attachment conical walls at the nozzle exit. The jet is switched between the walls by means of a control flow. The oscillating control action aims at utilizing the ordered vertical structures in the jet shear layer [11 and 17]. This method has been investigated by several authors; the most widespread variant being an application of acoustic excitation (as used also in the present research), the other methods using oscillating suction/blowing control flows or mechanical vibration. The oscillatory control action may be either forced externally (active control) or can be present without external forcing (passive control) either because of intrinsic instability of shear flows (self-sustained oscillations) or utilizing some of the principles of fluidic oscillators. A well known fact should be emphasized that the pulsation cannot be

always expected to enhance the heat transfer; there are cases where the effect has even lead to a decrease in performance—see [23].

Hwang et al. [22] investigated heat transfer of actively controlled axisymmetric impinging jet by means of an annular steady control jet (co-flowing or counter flowing) or by acoustic excitations. Frequency of the acoustic excitation was derived from the fundamental frequency of vortex generation, based upon the evaluated Strouhal number ≈1.2. The harmonic and double harmonic excitation caused promotion or suppression of the vortex pairing, and measurable enhancement or reduction in heat transfer, respectively. The region of maximum heat transfer was moved up- or downstream, respectively. Subsequently, Hwang and Cho [24] discussed the influence of the location where the acoustic input was applied—in particular they studied excitation of the main jet upstream from the nozzle (an approach comparable with the present one) and the shear layer excitation near the nozzle exit lip. Surprisingly, no significant influence of the location of the input effect could be identified from the both investigated points of view—flow characteristics (measured with hot-wire anemometer) and local heat transfer (evaluated from thermocouple measurements using a gold coated heated film). It is noteworthy that an azimuthally controlled acoustic excitation near a round nozzle lip gives many possibilities to control three-dimensional modes of large-scale vortex structures—see, e.g., experimental investigation by Corke and Kusek [25], and recent direct numerical simulation by Tsubokura et al. [14]. Lepičovský et al. [26 and 27] investigated round jets under strong upstream acoustic excitations (128–141 dB) at Strouhal number from 0.4 to 0.6. They found the upstream acoustic excitation essentially enhancing the turbulence intensity as well as the jet spreading rate and fluid mixing. These effects are very significant in the region close to the end of the jet potential core because of the enhanced generation of the large-scale structures there. This conclusion is in tune with earlier investigations focusing on acoustic modification of turbulent round jets by Vlasov and Ginevski [28 and 29]: the low frequency acoustic excitations at Strouhal NUMBER=0.2–0.6 causes an intensification of turbulence and mixing through promotion of large vortices; on the other hand, high frequency at Strouhal NUMBER=2–5 causes (through promotion of small vortices) a reduction of turbulence and mixing.

Cho et al. [30] investigated an axisymmetric jet under an acoustic two-frequency excitation and focused their attention on the control role of phase differences. They used flow visualization and velocity measurements, and found that stable vortex pairing can be controlled, and mixing rate can be substantially enhanced, by means of the fundamental frequency and its subharmonic forcing at the Strouhal number from 0.3 to 0.6. The value of 0.3 is in tune with the most preferred mode (i.e. the most amplified mode obtained by an artificial external excitation) according to Crow and Champagne [17]. Moreover, Cho et al. [30] observed a non-pairing advection of vortices for higher Strouhal number from 0.6 to 0.9. More recently, a round impinging jet under single as well as two frequency (fundamental and subharmonic) excitations was experimentally studied by Vejračka [31] at small nozzle-to-wall spacing (H/D=2), at Strouhal numbers from 0.56 to 2.4; he showed sensitivity of flow to (mainly two frequency) excitations, and a possibility to control vortex roll-up processes.

Gau et al. [32] investigated the acoustic control of impingement heat transfer and concluded that inherent frequencies enhance heat transfer through increased turbulence intensity, and non-inherent frequencies can reduce turbulent intensity and decrease heat transfer. Liu and Sullivan [33] investigated the heat transfer of an excited round impinging jet at relatively small nozzle-to-wall spacing ($H/D \lesssim 2$); having obtained an enhancement or reduction of the local heat transfer by controlling the vortex structure development by forcing near the natural frequency (Strouhal number ≈1.2) or its subharmonic, respectively.

It is already a known fact that impinging jets can exist in *several steady states* of the time-mean flow field, between which there are regimes in which the flow field behavior is *bistable* and sometimes even hysteretic in character. The bistability of impinging jets can be observed in cases with the jet split into separate branches by an insertion of an obstacle into the flow (annular or two-slot jets). The bistability results from interactions of the flow branches. Maki and Yabe [34] experimentally investigated an annular impinging jet, and identified four flow regimes of the flow field; three of these regimes were characterized as a recirculating unsteady flow. The other experimental study of the same authors was performed at relatively large inner diameter of annular nozzle, D_i/D_o=0.80 to 0.98 (Maki and Yabe [35]); they clarified (by means of pressure distribution on the wall, hot-wire measurement, and naphthalene sublimation technique) three flow field patterns, which existence was unambiguously determined by nozzle-to-wall distances.

Numerical study of Kokoshima et al. [36] of an annular impinging jet predicted a bistable behavior (the regimes differing in what they called a "closed" and "open" flow pattern) including a hysteresis. The phenomenon of bistability and hysteresis of impinging jets was investigated experimentally by Trávníček and Křížek [37] for the planar geometry (a two-dimensional impinging jet from a two-slot-nozzle, i.e. a slot nozzle which is divided into two halves by an inserted fixedpartition bar)—the paper [37] is probably the first publication describing this phenomenon in a reviewed journal. An advanced variant of the nozzle geometry has been studied by Trávníček and Marčík [38]. Recent study by Tesač et al. [39] involved annular impinging jets, in which five flow regimes were identified by a numeric simulation in association with hot wire measurements, including bistability on ademarcation boundary between two of them. No hysteresis was referred to in [39]—the phenomenon is, apparently, very complex and depends on a specific geometry. The other variant of an actively controlled, bistable annular impinging jet which can be switched by on/off fluidic control, has been studied recently by Trávníček et al. [16].

The previous paper by Trávníček and Tesač [40] revealed two states of an annular impinging (zero-net-mass-flux) synthetic jet (the paper [40] is probably the first publication on the synthetic impinging jets in a reviewed journal). One flow state is characterized by a relatively small recirculation bubble located just at the nozzle center body. It occurs at higher frequency, namely 693 Hz. The second flow state, with the bubble expanded into a large separated flow area reaching up to the impingement wall, was found at lower frequencies (106–263 Hz). In other words, the two alternative, essentially different states of the time-mean flow field have been obtained by means of the choice of the excitation frequency under identical geometry conditions.

To the best of the present authors' knowledge, no other similar switching of the time-mean flow in a jet impingement by means of an acoustic control has ever been discussed in available literature. It is suggested that this switching effect can be useful for the desirable enhancement of the heat transfer. Therefore, the periodically excited impinging jets with actively controlled time-mean flow field state, namely the annular impinging jets whose central recirculation zone (bubble) is acoustically controlled, seem to be a very promising alternative for various heat transfer applications. These are the main motivations for a study of this subject, and the present experimental paper is an initiation step of such investigation.

2. Experimental facilities and techniques

Flow visualizations and mass transfer experiments described in this paper were made using the annular nozzle as shown in Fig. 1. The present experiments represent a continuation of the previous investigation by Trávníček and Tesař [40], which was dealing with annular zero-net-mass-flux synthetic impinging jet. This means that no steady flow air supply was used in [40], and the resultant synthetic jet has been generated (or synthesized) exclusively from the outer air by the periodic actuations (description of synthetic jets, e.g., [41], and recently [42]).
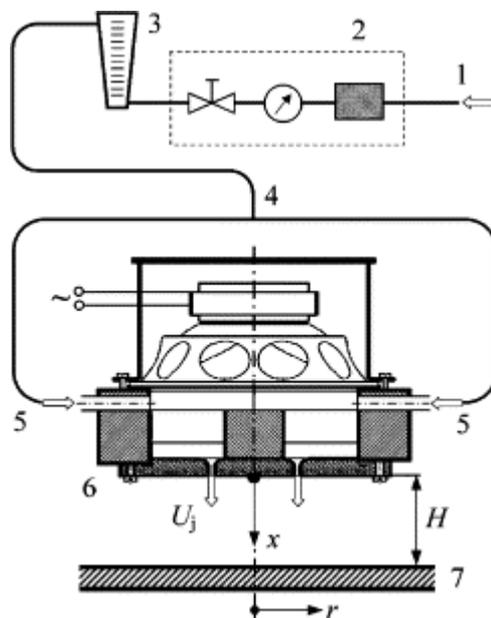

Fig. 1. Annular nozzle with an acoustic excitation. 1: Air flow supply, 2: filter and pressure regulator, 3: rotameter, 4: flexible tubing, 5: pair of input radial channels, 6: annular nozzle equipped with the loudspeaker, 7: exposed wall.

The present nozzle is practically identical with that described in [40], the only difference being the pair of the air supply channels—see Fig. 1. The air flow is supplied by a compressor and kept constant by pressure regulator. The flow rate is measured by the rotameter (LABORATORNÍ PŘÍSTROJE, type 60, Prague)—see schematic diagram in Fig. 1. The air flow passes through a flexible plastic tube of inner diameter and length 10 mm and about 5 m, respectively. This tube is connected

via T- adaptor to both input channels of the nozzle. The inner and outer exit diameters or the nozzle are D_i=38.0 mm and D_o=40.0 mm, respectively; (representing the diameter ratio D_i/D_o=0.95). The nozzle is equipped with the loudspeaker of 100 mm diameter (TESLA ARN 100 10/4), supplied by sinusoidal driving current of adjustable frequency. The nozzle is positioned vertically, the nozzle axis is directed downwards. For study of the jet impingement, a horizontal plane wall is inserted below the nozzle exit. The wall for visualization is made of plywood, covered with plastic black foil. The wall for the mass transfer experiments is covered with a layer of naphthalene. Investigated nozzle-to-wall spacings were H/D_o=0.50, 0.75 and 1.00; this choice covers an expected location of the point of the reattachment of annular (non-impinging) jets (e.g., [43 and 44]). The trend of the reattachment distance with the diameter ratio D_o/D_i was originally presented in graphical form by Ko and Chan [43]; it can be correlated here as

$$x_r/D_o=2.76D_o/D_i-2.12. \tag{1}$$

This expression results for the present nozzle in $x_r/D_o\approx0.79$ (i.e., $x_r\approx31$mm). Moreover, the present investigated H/D_o—range covers the expected "critical value" of the nozzle-to-wall distance, where two of the most distinctive states of annular impinging jets border on each other: according to Maki and Yabe [35], the change from the small to the large recirculation zone as well as back from large to small ones (no hysteresis were referred in [35]) is unambiguously determined by the correlation equation, which after simple algebraic modification yields

$$x_c/D_o=-5.35(D_o/D_i-1)^2+5.2(D_o/D_i)-4.497. \tag{2}$$

This correlation results for the present nozzle in $x_c/D_o\approx0.91$ (i.e., $x_c\approx37$ mm).

The present experiments were performed in a test chamber (width 1,3 m × depth 0,8 m × height 1,8 m), well ventilated to the outside of the laboratory (because of naphthalene experiments). Thick glass–fiber curtain around the chamber (except for an observation window) effectively avoided direct reflection of the sound into the flow field.

Sound pressure level (SPL) was measured by means of the Sound Level Meter QUEST210 (Frequency Weighting Networks A, which emulates the low level response of the human ear), with its microphone (dia. 13.5 mm) located perpendicularly to the nozzle axis in the point of x=10 mm, r=40 mm.

The smoke-wire technique was used for the visualization of air jet downstream from the nozzle. Similarly as in [16 and 40], the smoke-wire was made from three resistance wires of 0.1 mm diameter, which were uniformly twisted together to increase the surface and to prolong the observation time. The smoke-wire was coated by paraffin oil before each test, and heated by Joule effect of DC current. Photographs of the resultant white streaklines on black background were taken by digital camera (Olympus C-2500L Camedia). The illumination was alternatively by (1) a continuous bulb light, or (2) instantaneous flashlight, or (3) stroboscope light (Cole-Parmer U-87002) synchronized with the excitation frequency.

Local mass transfer was measured by using the naphthalene sublimation technique. This was described exhaustively by Goldstein and Cho [45]; the authors' present variant, which originates from work by Korger and Křížek [46], was described recently [40]. The local mass transfer coefficient is calculated from the sublimation depth Δx as

$$h_{\mathrm{m}} = \frac{\rho_{\mathrm{n}} R_{\mathrm{naph}} T_{\mathrm{w}} \Delta x}{p_{\mathrm{sat}} \Delta t}.$$
(3)

where ρ_{n} is the density of solid naphthalene, (ρ_{n}=1175 kg/m^3 at 20 °C), R_{naph} is the gas constant of naphthalene vapour (R_{naph}=64.87 J/(kg K)), T_{w} is the absolute temperature of the exposed surface, Δx is net local sublimation depth, p_{sat} is the saturated vapor pressure of naphthalene at the surface temperature (calculated from the empirical equation by Ambrose et al. according to a recommendation [45]), and Δt is the run duration. The extraneous sublimation due to natural convection has been evaluated by an auxiliary experiment—the resultant correction of the h_{m}—value was 0.0023 m/s. The maximum sublimation depth was 0.1 mm, the run duration time was 45–90 min.

Non-dimensional expression of mass transfer coefficient is the Sherwood number, $Sh=h_{\mathrm{m}}D_{\mathrm{o}}/D_{\mathrm{naph}}$, where D_{naph} is the mass diffusion coefficient of naphthalene vapor in air, calculated for measured temperature of the jet, and from barometric pressure [45]. Based on the heat/mass transfer analogy [45], the mass transfer data can be converted to the corresponding heat transfer data by the following relation

$$Sh/Sc^n = Nu/Pr^n,$$
(4)

where Sc, Nu, and Pr are Schmidt, Nusselt, and Prandtl numbers. The range of the exponent n is 0.33–0.42 (e.g., the n=1/3 on a flat plate in laminar flow), and its value may be determined from empirical results [1, 2 and 45]. The present mass transfer data are processed by using n=0.4, which is a commonly accepted value for turbulent impinging jets [1 and 45]. The Sc is calculated for measured air temperature from empirical equation [45]; the typical value is 2.28 at 25 °C.

Two thermistor probes, connected with THERM 2280-3, were used to measure air temperature, one located in the ambient air, the other one inserted into the nozzle exit before each test run, to make sure that the experiments are made after required temperature equalization. The temperature range was from 21.1 to 23.2 °C for all experiments.

Uncertainty analysis was performed according to Kline and McClintock's method [47] for single sample experiment. The uncertainty of the solid naphthalene density ρ_{n} temperature T_{w} sublimation depth Δx, duration of test run Δt, nozzle diameter D_{o}, saturated vapor pressure p_{sat} and mass diffusion coefficient D_{naph} were estimated to be 1.1%, 0.06%, 4.3%, 0.5%, 0.1%, 3.77%, and 5.1%, respectively. The uncertainty of the mass transfer coefficient and the Sherwood number is within 6% and 9% in the entire range of measurements based on a 95% confidence level (±2 standard deviation).

3. Results and discussions

All experiments with acoustically excited annular jet, described in the present paper, were made at the constant volume flow rate 0.00137 m^3/s, i.e. at the average exit velocity from the nozzle U_J=11.2 m/s. Also constant was the input electrical power 4.0 W supplied into the loudspeaker. Four frequencies of the acoustic excitation are discussed here, namely f=106, 155, 263 and 692 Hz.

A description in dimensionless form such as Reynolds and Strouhal numbers requires using of *adequate* characteristic length scales. However, for the present complex (or multi-scale) problem of an annular jet, a choice of a characteristic length scale is rather questionable.

It is well known fact that even for a simple slot (or round) fluid jets, two length scales are necessary to be taken into account, namely the initial boundary layer thickness at the nozzle, and the jet transversal dimension (width or diameter). The former is important for a development and instability of the jet shear layer near the nozzle lip at shear-layer mode of coherent structures, and the latter is relevant to a development and instability of entire jet at the jet-column mode—see, e.g., [17, 18, 29 and 48]. An annular jet is more complex, thus an additional length scale is necessary to be taken into account. Typically, the outer diameter of the annular nozzle, D_o, is employed in definition of Strouhal number—e.g., [43 and 49].

In the present geometry, the annular slot is very narrow (B/D_o=0.025). The boundary layer thickness, and the annular slot width B can be considered characteristic length scales for a development and instability near the nozzle lip. However, the present work focuses on a development of an entire annular jet, especially on the behavior of a recirculation zone (bubble). Apparently, an *adequate* length scale should be in tune with the size of this large scale structure.

As a result of these considerations, and because of comparison purposes with the existing other publications, Reynolds and Strouhal numbers are defined alternatively in the present paper by using two length scales: annular slot width B(Re_B=U_JB/ν ,St_B=fB/U_J), and annular nozzle diameter D_o (Re=U_JD_o/ν,Sh=fD_o/U_J). The former length scale B can be useful for description of the narrow annular slot jet including its active control, and the latter length scale D can be useful for a behavior of entire recirculation zone (bubble) including its active control (which is the aim of this work).

The Reynolds numbers of experiments are Re=28 600, Re_B=715. Investigated four frequencies of the acoustic excitation (f=106, 155, 263 and 692 Hz) correspond to Strouhal numbers Sh=fD_o/U_J=0.38, 0.55, 0.94, and 2.47, and Sh_B=fB/U_J=0.0095, 0. 014, 0.023, and 0.062, respectively. This choice of frequencies is in agreement with an expected response of the jet to an external excitation.

The highest sensitivity of round jets to excitation (i.e. the most amplified mode under small artificial excitations) is known be at the most preferred mode, at Strouhal number of 0.3–0.35 [17]. As mentioned above, the situation in annular jets is governed by two scales, e.g., Strouhal numbers for intermediate merging zone of the outer mixing region of annular jets are comparable or slightly smaller than those of

round jets, a very gradual decrease around 0.35 was presented, e.g., by Chan and Ko [49]. (However, their results relate to rather small ratio of diameters D_i/D_o=0.45 unlike the present D_i/D_o=0.95.) The lower boundary of our experimental range, Sh=0.38, is very close to these values. However, Strouhal number of the jet column mode of round jet themselves (natural passage frequency of vortices without any artificial excitation) is higher, e.g., about 0.5 by Crow and Champagne [17], 0.61 by Liu and Sullivan [30]; moreover much wider range is possible from 0.25 to 0.85 according to Thomas [48]—who discussed an essential influence of the thickness of the boundary layer at the nozzle output. Our chosen values Sh=0.55 and 0.94 correspond to this range of frequencies. Finally, the highest chosen frequency, Sh=2.47, was inspired by a successful experiment by Hwang et al. [22]. They used, among other means, an acoustic excitation of their round impinging jet at Sh=2.4, which was the double harmonic of the fundamental frequency of vortex generation, and this was found to suppress the vortex pairing and moved a region of maximum heat transfer further downstream.

A few experiments were made at the same Re without excitation for comparison purposes. Other comparisons were made with zero-net-mass-flux annular impinging synthetic jets, which have been studied recently by Trávníček and Tesař [40].

Sound Pressure Level, SPL, of annular jet without excitation and without exposed wall was 73.8 dB. Because of the reflection of the sound from the exposed wall, SPL increases with the jet impingement, and with decreasing nozzle-to-wall spacing: SPL of the annular impinging jet without excitation was 96.5, 98.6 and 98.7 dB for H/D_o=1.00, 0.75 and 0.50, respectively.

The SPL of an acoustically excited annular jet increases monotonically with the frequency. For non-impinging jets, the SPL increases from 76.6 dB to 99.9 Hz for f=106–692 Hz, respectively. The impingement wall reflects the noise, thus SPL for impinging jet increases from 99 ± 2 dB to 125 ± 2 Hz for f=106–692 Hz, respectively. In the present range of the nozzle-to-wall spacing, SPL varies only insignificantly. This is the reason for the value of the range given as ±2 dB (understandably, lower SPL values are valid for larger H/D_o=1.00, and vice versa). This increase of the excitation amplitude with frequency is caused by the resonance in the settling chamber upstream from the nozzle, and by the frequency dependence of the loudspeaker itself. This is the common feature (and disadvantage) of this method of frequency response investigation based on constant input power—cf. e.g., [27]. In contrary, the other method lies in keeping SPL constant by means of input power variation—see, e.g., [22].

3.1. Flow visualization

The basic phenomena in the acoustically excited annular jet were qualitatively studied by means of smoke visualization. Fig. 2 shows this visualization at Strouhal number Sh=0.38 (i.e., f=106 Hz). Fig. 2(a) shows the time-mean flow field—a photograph of long (1 s) exposure over a large number of cycles. The formation of individual large-vortex structures is shown by means of an instantaneous streaklines photograph taken as a single short exposure in Fig. 2(b). Fig. 2(c) shows multiple exposure of 106 superimposed frames, which were taken at instants phase-locked to the beginning of the excitation cycle; the photo shows the mean streaklines, smoothing out the

fluctuation deviations of individual cycles. The photographs in Fig. 2 demonstrate quite well the symmetry of the jet, and also the single large-scale toroidal vortex structure near the nozzle exit (located approximately at $x=0.7D_o$ at the beginning of the excitation cycle—see Fig. 2(c)). This behavior is qualitatively similar to the previously investigated annular synthetic jet by Trávníček and Tesař [40]. Understandably, a distance of this structure from the nozzle is distinguishably larger now, because the structure is moved further downstream by the time-mean flow component, approximately by 40% to 60% relatively to the zero-net-mass-flux synthetic jet.
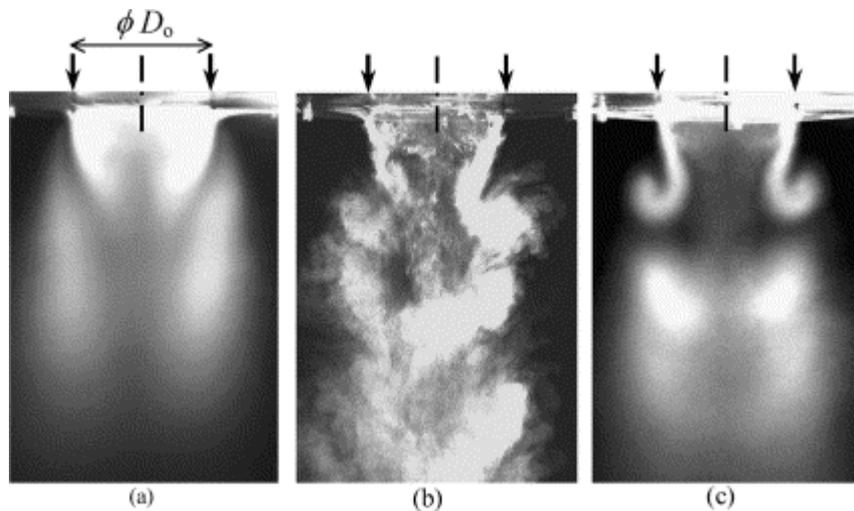

Fig. 2. Smoke visualization of the annular jet at $Sh=0.38$ (i.e., $f=106$ Hz): (a) time-mean flow field under a continuous exposure during 1 s; (b) instantaneous streaklines under a single flash exposure; (c) multiple exposure of 106 frames, which were phase-locked taken at the beginning of the excitation cycle.

The influence of the excitation frequency on this structure formation is shown in Fig. 3 at $Sh=0.38$, 0.55, and 0.94 ($f=106$, 155, 263 Hz). The distance structure-to-nozzle decreases monotonically with increasing frequency from $x/D_o=0.7$ to 0.2 at $f=106$–263 Hz. A similar tendency, but with the distances increased by 40%–60% was identified in the synthetic jets during previous investigations [40].
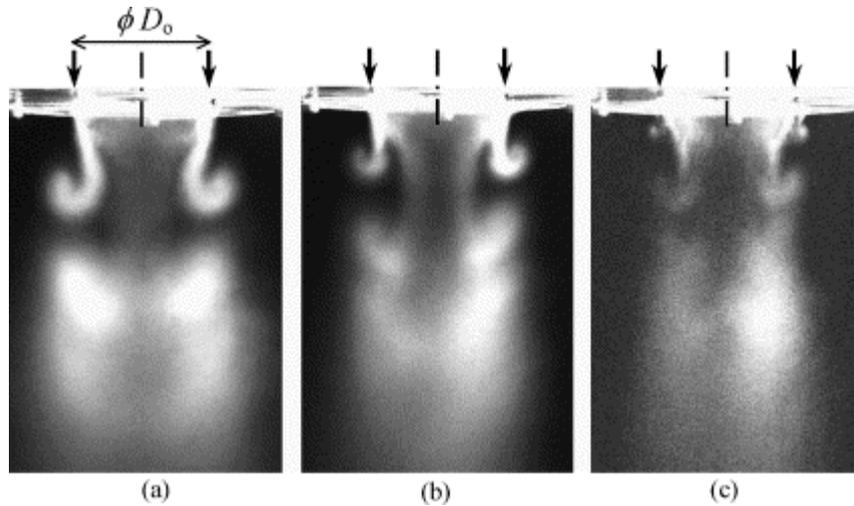
Fig. 3. Effect of excitation frequency on a location of the large-scale vortex structure. The photos are multiple exposures during 1 s, which were phase-locked taken at the beginning of the excitation cycle; (a) Sh=0.38 (f=106 Hz); (b) Sh=0.55 (f=155 Hz); (c) Sh=0.94 (f=263 Hz).

Fig. 4 shows visualization of the annular jet impingement at Sh=0.38. The large toroidal structure is well visible under the multiple exposition conditions in Fig. 4(b). This structure is pressed upstream by the impingement wall, approximately by 30% in comparison with non-impingement case of Fig. 2. Moreover, the jet impingement apparently enhances some asymmetry of flow field. This asymmetry is undoubtedly the reason for the asymmetry of mass-transfer profiles, discussed later.
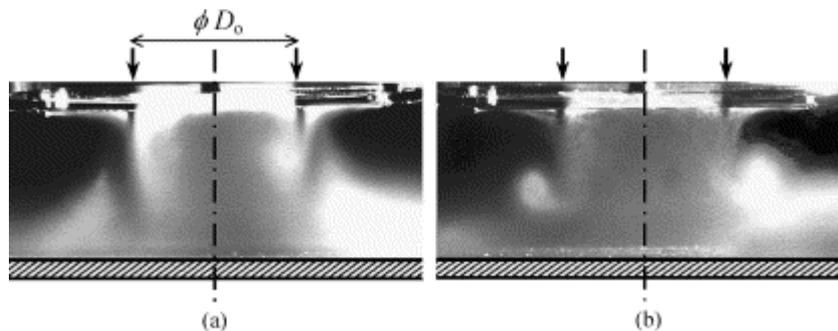

Fig. 4. Annular impinging jet at Sh=0.38 (f=106 Hz): (a) time-mean flow field under a continuous exposure during 1 s; (b) multiple exposure of 106 frames, which were phase-locked taken at the beginning of the excitation cycle.

Two expected states of investigated flow field are drawn schematically in Fig. 5. These ideas about the flow field are based on known information about steady annular impinging jets, e.g., by Maki and Yabe [34 and 35], Kokoshima et al. [36], Trávníček et al. [16], and Tesař et al. [39]:

• Annular impinging jet in state 1, see Fig. 5(a): *the small recirculation zone (bubble) of separated flow, which is located just behind the nozzle center body*. The central

stagnation point exists at the point of intersection of the nozzle axis with the wall, and no other stagnation points are on the wall. Maximum heat/mass transfer is achieved at the central single stagnation point, the heat/mass transfer profiles are bell-shaped. The flow field near this stagnation point qualitatively resembles the basic case of a round impinging jet—streamlines on the exposed wall run away from the central stagnation point. Therefore, this state has been called the "centrifugal case" by Tesař et al. [39]. Another name, the "closed type pattern", was referred to by Kokoshima et al. [36].
• Annular impinging jet in state 2, see Fig. 5(b): *the large recirculation zone* of separated flow reaches up to the impingement wall. Entire nozzle-to-wall space is filled up with the separation region flow. This state is referred to as the "open type pattern" by Kokoshima et al. [36], or the "reverse stagnation point" by Maki and Yabe [34 and 35]. Recently, this flow pattern has been called more aptly as the "centripetal case" by Tesař et al. [39]—since the wall streamlines run from an outer stagnation circle towards the central, reverse stagnation point. Maximum heat/mass transfer is achieved on the stagnation circle.
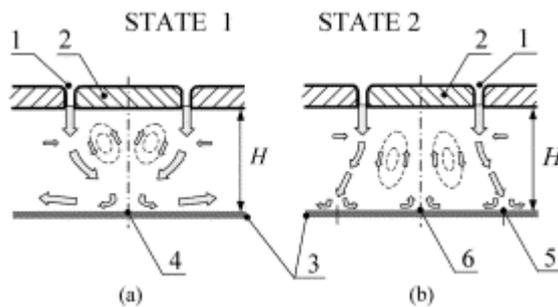

Fig. 5. Scheme of two states of the annular impinging jet, (a) state 1—small central recirculation zone (bubble), (b) state 2—large central recirculation zone. 1: Annular slot of the nozzle, 2: central body, 3: exposed wall, 4: central stagnation point, 5: stagnation circle, 6: reverse stagnation point.

States 1 and 2 are typically and primarily linked with larger and smaller nozzle-to-wall spacings, respectively. However, due to a bistability and hysteresis, sometimes either the state 1 or the state 2 can exist at the some geometry [16, 36 and 37]. This means that the actual state at the bistability depends not only upon the instantaneous parameters, but on the previous set-up history as well.

3.2. Mass transfer experiments

Fig. 6 shows an example of the mass transfer measurement at Strouhal number Sh=0.94 (f=263 Hz), and at the nozzle-to-wall distance H=1.0D_o. The lines plotted in Fig. 6 are the lines of constant time-mean mass transfer in non-dimensional form of Sherwood number, Sh. The highest values of the mass transfer coefficient are on the stagnation circle (broken circle line in Fig. 6) the diameter of which is 1.36D_o. Evidently, the annular impinging jet is in the state 2—the large recirculation zone. Almost circular character of the lines in Fig. 6 gives an idea of the symmetry of the experiment. Some azimuthal variations are probably due to some geometry inaccuracy; which is extremely difficult to avoid, given the high sensitivity as will be discussed in association with Fig. 7 below.
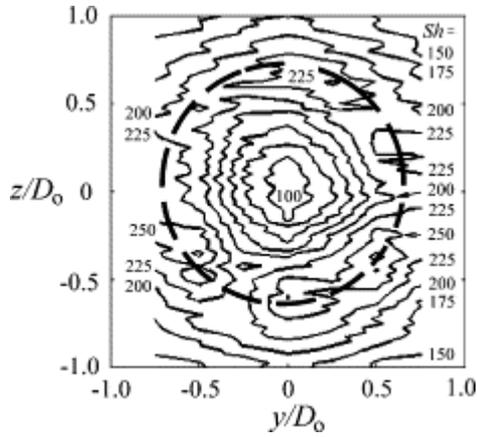
Fig. 6. Distribution of mass transfer onto exposed wall as constant Sherwood number lines. Steps between Sw-lines are 25, H=1.0D_o, the broken circle line shows the stagnation circle.
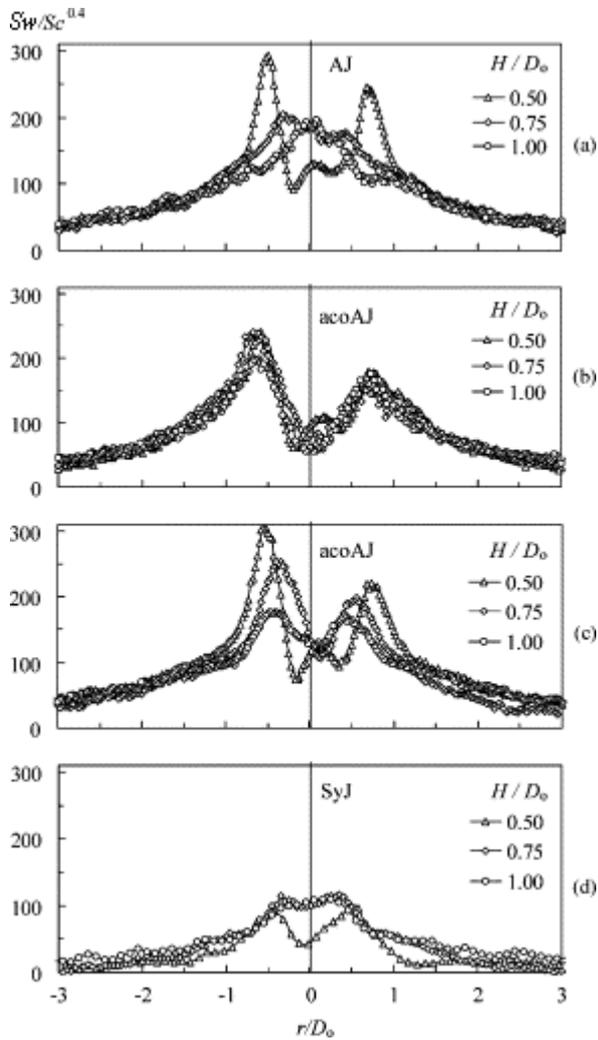

Fig. 7. Distribution of the local mass transfer onto wall in terms of radial distributions of Sherwood number Sw : (a) AJ-annular impinging jet; (b) acoAJ-acoustically excited annular impinging jet at Sh=0.94 (f=263 Hz) and (c) Sh=2.47 (f=692 Hz); (d) SyJ-annular impinging synthetic (zero-net-mass-flux) jet at f=692 Hz.

Fig. 7 presents the mass transfer experiment at the distances H/D_o=0.50, 0.75 and 1.00 for non-excited as well excited annular jets, noted as AJ and acoAJ, respectively. For comparison purposes, the mass transfer of annular impinging synthetic jets (noted SyJ in short) at identical geometry is also shown in Fig. 7(d). The change of the mean-flow field state, which results from different excitation frequencies, is demonstrated rather well there. Fig. 7(a)–(d) confirm the understandable fact that all jets (AJ, acoAJ, SyJ) at the small nozzle-to-wall distances H/D_o=0.5 exhibit the large recirculation zone (state 2), which fills up completely the nozzle-to-wall space, and which produces the stagnation circle of maximum mass transfer on the wall. On the other hand, the flow field situation at larger nozzle-to-wall distances is much more complicated, and it essentially depends on the excitation frequency:

Fig. 7(a) shows that non-excited annular jets at the largest distance H/D_o=1.00 has the small recirculation zone (bubble; state 1). The medium distance, H/D_o=0.75, is related to a rather unstable flow field behavior with a non-typical mass transfer profile, when neither the stable single central stagnation point nor stable circle stagnation line are distinguishable. Present time-mean mass transfer experiment manifests this behavior by the relatively large central stagnation area (about 0.7 D_o in diameter).

Fig. 7(b) shows that excitation at Sh=0.94 stabilizes very well the large recirculation zone. An increase of the nozzle-to-wall distances in the present range from H=0.50 to 1.00 practically does not change the stagnation circle, which is about 1.36 D_o in diameter. Moreover, mass transfer of this well stabilized flow field is nearly independent on H-distances.

Fig. 7(c) shows that excitation at the highest tested frequencies, Sh=2.47, (f=692 Hz), cannot stabilize the large recirculation zone as efficiently as the previous case of Sh=0.94. An increase of H-distances causes a gradual decrease of the recirculation region, namely the decrease of the stagnation circle size. Evidently, this behavior manifests a tendency to change the large recirculation zone into the small bubble at increasing H, similarly as is the case for AJ in Fig. 7(a). On the other hand, although the size of the large recirculation zone decreases now, the excitation at Sh=0.94 is still efficient enough to prevent the collapse of this zone into state 1.

For a comparison, Fig. 7(d) shows the mass transfer experiment of the annular impinging synthetic jet (SyJ) at f=692 Hz, i.e., at the same frequency as acoAJ in Fig. 7(c). It is evident that SyJ at the smallest distance H/D_o=0.50 is in the state 2 (the same behavior as acoAJ), but at the larger H/D_o=1.00 the SyJ is in state 1—unlike the state 2 of acoAJ. In fact, this behavior is linked with the relatively high excited frequency 692 Hz. It is a known fact that SyJ at lower frequencies 106–263 Hz exhibit only large recirculation zones at all these distances H/D_o=0.50–1.00 (see [37]). Now, the present experiments clearly show that acoAJ can be much better stabilized into the state 2 at larger distances H=1.00D_o than the SyJ (comparison of Fig. 7(c) and (d)), as well as than AJ (comparison of Fig. 7(c) and (a)). The comparison of acoAJ with SyJ is in agreement with the flow visualizations mentioned above: The distance of the large toroidal vortex structure from the nozzle is distinguishably larger for the acoAJ, because this structure is moved further downstream by the mean flow.

The difference between the two halves of the profiles in Fig. 7 gives an idea about the achievable symmetry of the flow field. The asymmetry of these mass-transfer profiles

are caused by the asymmetry of impinging jet, mentioned above—see visualization in Fig. 4. The main reason is probably the extreme sensitivity of the present flow field to the accuracy of geometry set-up, particularly conditioned by the occurrence of an instability. This instability (or bistability) emerges from an existence of the two flow states, 1 and 2. Therefore, annular impinging jets are much more sensitive to perturbation influences, including inaccuracy and even slight deviations from the ideal axisymmetric geometry, than non-impinging jets. The jet impingement amplifies any inaccuracy of the flow field set-up. Flow visualization presented above qualitatively supports this opinion: the non-impinging jet in Fig. 2 demonstrates a reasonable symmetry, unlike the impinging jet in Fig. 4, the asymmetry of which is evident in spite of the same geometry of the nozzle. Accuracy of the geometry was evaluated by an auxiliary measurement; an error of adjustment of the annular nozzle width was evaluated to be about ±0.02 mm (this is apparently a not negligible value, especially for the present very sensitive flow field near bistability).

In the following text, the mass transfer profiles are evaluated by averaging the both halves of individual experimental profiles. This data processing is considered valuable for a clear explanation of results, because smoothing of some irregular deviations allows focusing on the essential subject: the acoustic control of the recirculation zone. Therefore, only right halves of graphs are plotted in the following Fig. 8 and Fig. 9.
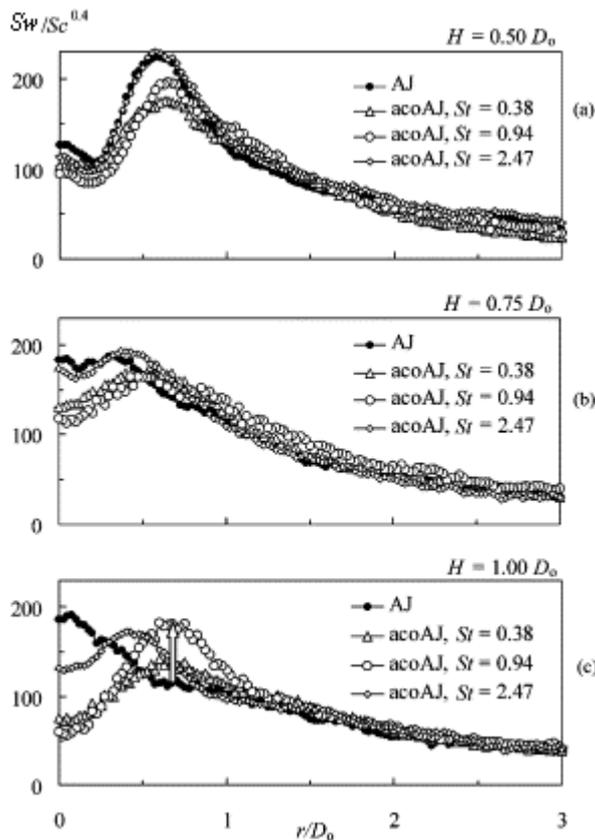

Fig. 8. Effect of acoustic excitation at different nozzle-to-wall distances. (a) H/D_o=0.50, (b) H/D_o=0.75, (c) H/D_o=1.0; the arrow shows enhancement of local mass transfer, which has been achieved by the acoustic excitation at Sh=0.94 in the stagnation circle over non-excited AJ.
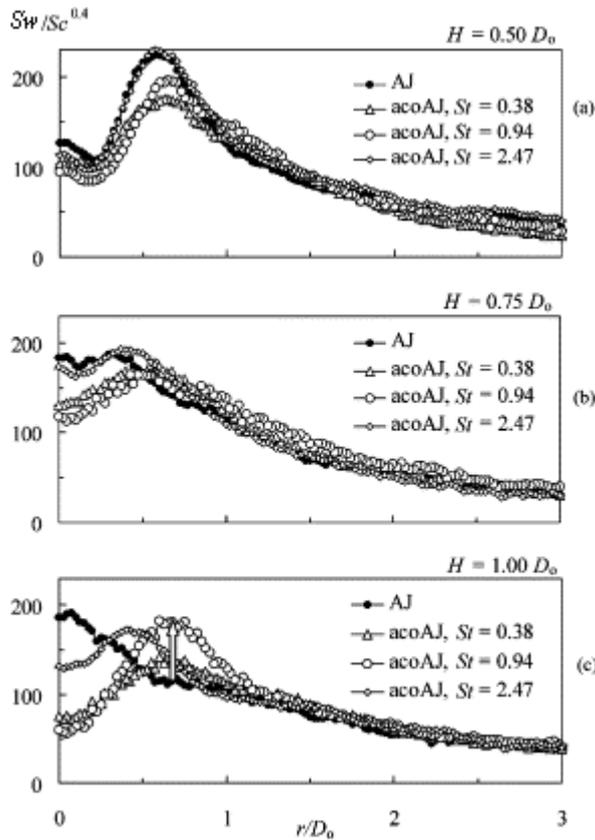
Fig. 9. Average mass transfer at the nozzle-to-wall distance H/D_o=1.0. The arrow shows enhancement of average mass transfer, which has been achieved by the acoustic excitation at Sh=0.94 over non-excited AJ.

Fig. 8 demonstrates an effect of the acoustic excitation at different nozzle-to-wall distances. Fig. 8(a) shows this effect at the smaller distance, H/D_o=0.5: Only the large recirculation zone (state 2) exits. Excitation at the highest frequency (Sh=2.47, f=692 Hz) has a practically negligible effect, and all lower frequencies decrease the mass transfer.

Fig. 8(b) shows effect of the acoustic excitation at the medium distance, H/D_o=0.75. Non-excited annular jet AJ is unstable and exhibits an atypical mass transfer profile with relatively larger central stagnation area of about 0.7 D_o in diameter, as discussed above at Fig. 7(a). An excitation at all frequencies stabilizes the large recirculation zone. The highest frequency (Sh=2.47) changes the mass transfer only moderately. All lower frequencies decrease the mass transfer in the central portion inside the stagnation circle, and slightly increase it at larger radii, approximately for r>0.6D_o.

Fig. 8(c) shows the most interesting results of the excitation effect, which is related to the larger tested distance, H/D_o=1.00. Non-excited annular jet AJ exhibits the state 1 with maximum mass transfer in the central stagnation point and approximately bell shaped Sh-profile. An excitation at whichever frequency turns the jet into state 2. This change is linked with a rather big decrease of the mass transfer in the center, and some increase in the size of the stagnation circle. In other words, the change from state 1 to 2 causes spreading of mass transfer onto a larger surface area. This effect is smaller at

the highest tested frequency, Sh=2.47. The highest mass transfer on the stagnation circle has been achieved at Sh=0.94, i.e., at the best stabilization of the large recirculation zone—see Fig. 7(b) above.

Let us compare the two most characteristic profiles of Sherwood number Sw in Fig. 8(c) at states 1 and 2, namely AJ and acoAJ at Sh=0.94, respectively. Mass transfer of acoAJ on the axis (there is the reverse stagnation point) is only 32% of the value of AJ. On the other hand, the comparison at the stagnation circle of acoAJ (about r=0.68D_o) shows a gain of acoAJ about 57%. This gain is indicated in Fig. 8(c) by the arrow. The maximum in the central stagnation point of AJ is slightly higher than the maximum on the stagnation circle of acoAJ (by approximately 5%). Despite this fact, a benefit is evident of the stagnation circle of acoAJ against the single stagnation point of AJ from the heat/mass transfer point of view. There is an obvious increase which results from the spreading of heat/mass transfer onto the larger surface area. To quantify this improvement, the local mass transfer values were integrated, and the average mass transfer along the surface in form of the average Sherwood number was evaluated as

$$\overline{Sw(R)} = \frac{1}{R^2} \int_0^R r \cdot Sw(r)\, dr$$

(5)

According to this definition, the local mass transfer data from Fig. 8(c) were recalculated and the result is plotted in Fig. 9 at the same radial coordinate, r=R. Now, a similar comparison of two the most characteristic profiles (AJ in state 1 with acoAJ at Sh=0.94 in state 2) can be made. The highest benefit of acoAJ over AJ is achieved at r=0.95D_o, when the average mass transfer of acoAJ is higher by 23%. This results is shown in Fig. 9 by the arrow.

Finally, it should be underlined that the present experimental mass transfer data can be understood at the same time as heat transfer prediction through the analogy of Eq. (4). For local and average heat/mass transfer, Eq. (4) gives $Nu/Pr^{0.4}$=$Sw/Sc^{0.4}$.

4. Conclusions

An acoustically excited annular impinging jet with ratio of diameters D_i/D_o=0.95 was experimentally investigated by means of flow visualization and wall mass transfer measurements. For comparison, a non-excited steady jet and a synthetic (zero-net-mass-flux) jet were also tested. The time-mean flow field exhibits two different states, either one with small recirculation zone (bubble) just downstream from the nozzle center body, or one with large recirculation zone that fills up the whole nozzle-to-wall space. The former state exhibits the central single stagnation point on the axis, the latter one exhibits the stagnation circle on the wall. Both states are primarily linked with the larger and smaller nozzle-to-wall spacings, respectively. However, the present work has proved that the conversion between the two states can be made under identical geometry conditions just by acoustic excitation.

For smaller nozzle-to-wall spacing, $H \lesssim 0.5D_o$, all jets—the unexcited, excited, and the synthetic one exhibit the large recirculation zone. On the other hand, the flow field at the larger nozzle-to-wall distances is quite more complicated, and it essentially depends on the excitation. For the largest of the investigated nozzle-to-wall spacing, $H=1.0D_o$, the recirculation zone of an unexcited jet cannot reach the impingement wall so that the separation region collapses into the small bubble. However, an acoustic excitation under identical geometry conditions can cause it to switch into the large zone. This switching was confirmed in the whole investigated range of frequencies at Strouhal number $Sh=0.38$ to 2.47.

Heat/mass transfer effects are quantified by using local and average mass transfer coefficients, when the naphthalene sublimation technique is employed. The distribution of the local heat/mass transfer along the radius for the small recirculation zone conditions is bell shaped, with the maximum in the central stagnation point, similarly as for a conventional round impinging jet. On the contrary, the large zone causes the single central stagnation point to expand into the stagnation circle and to spread the heat/mass transfer on a larger surface area. The consequent enhancement of the average heat/mass transfer is significant and may be utilized in various impinging jet applications.

• Of primary interest in this paper is the large recirculation zone and the possibility of forcing the flow field into this state by means of an acoustic excitation. The described experimental confirmation of this possibility is the first main result of this study: The best stabilization of the large recirculation zone has been achieved at $Sh=0.94$.
• The second remarkable result is the significant enhancement of the average heat/mass transfer, which was achieved through the stabilization of the large recirculation zone the same $Sh=0.94$. The improvement through the acoustic excitation was 23% on the area of averaging radius $0.95D_o$, at nozzle-to-wall spacing $H=1.0D_o$.

It should be emphasized that heat/mass transfer enhancement is very desirable for many engineering applications. The present paper demonstrates a simple way how to achieve a remarkable improvement. Apart from this practical aspect, the prime results of this work, namely the suggestion and the experimental confirmation of the acoustic control of time-mean flow field, is considered to be of more general importance. Obviously, these effects are linked with behavior of large-scale structures in the impinging jet. A better understanding of the control mechanisms will require further systematic studies of fluid dynamics of these structures and their active control, as well as subsequent studies of heat/mass transfer enhancement under these conditions. Present experimental work, which demonstrates this possibility, is considered to be the initial step for the future studies.

Acknowledgements

References

1. E.P. Dyban and A.I. Mazur, Konvektivnyj teploobmen pri strujnom obtekanii tel. , Naukova dumka, Kiev (1982) (in Russian) .

2. H. Martin, Heat and mass transfer between impinging gas jets and solid surfaces. *Adv. Heat Transfer* **13** (1977), pp. 1–60.

3. S.J. Downs, E.H. James, Jet impingement heat transfer—a literature survey, in: Proceedings of the National Heat Transfer Conference, ASME, Pennsylvania, PA, 1987, 87-HT-35

4. K. Jambunathan, E. Lai, M.A. Moss and B.L. Button, A review of heat transfer data for single circular jet impingement. *Int. J. Heat Fluid Flow* **13** 2 (1992), pp. 106–115.

5. R. Viskanta, Heat transfer to impinging isothermal gas and flame jets. *Exp. Therm. Fluid Sci.* **6** (1993), pp. 111–134.

6. S. Polat, Heat and mass transfer in impinging drying. *Drying Technol.* **11** 6 (1993), pp. 1147–1176.

7. B.W. Webb and C.-F. Ma, Single-phase liquid jet impingement heat transfer. *Adv. Heat Transfer* **26** (1995), pp. 105–107.

8. S.V. Garimella, Heat transfer and flow fields in confined jet impingement. *Ann. Rev. Heat Transfer* **11** (2000), pp. 413–494.

9. C. Meola, G. Cardone, C. Carmicino, G.M. Carlomagno, Fluid dynamics and head transfer in an impinging air jet, in: Proceedings of the 9th International Symposium on Flow Visualization, Edinburgh, UK, 2000, No. 429

10. A.S. Fleischer, K. Kramer and R.J. Goldstein, Dynamics of the vortex structure of a jet impinging on a convex surface. *Exp. Therm. Fluid Sci.* **24** (2001), pp. 169–175.

11. J. Sakakibara, K. Hishida and W.R.C. Phillips, On the vortical structure in a plane impinging jet. *J. Fluid Mech.* **434** (2001), pp. 273–300.

12. M. Fairweather and G.K. Hargrave, Experimental investigation of an axisymmetric, impinging turbulent jet. 1. Velocity field. *Exp. Fluids* **33** (2002), pp. 464–471.

13. M. Angioletti, R.M. Di Tommaso, E. Nino and G. Ruocco, Simultaneous visualization of flow field and evaluation of local heat transfer by transitional impinging jets. *Int. J. Heat Mass Transfer* **46** 10 (2003), pp. 1703–1713.

14. M. Tsubokura, T. Kobayashi, N. Taniguchi and W.P. Jones, A numerical study on the eddy structures of impinging jets excited at the inlet. *Int. J. Heat Fluid Flow* **24** 4 (2003), pp. 500–511.

15. N. Gao, H. Sun and D. Ewing, Heat transfer to impinging round jets with triangular tabs. *Int. J. Heat Mass Transfer* **46** 14 (2003), pp. 2557–2569.

16. Z. Trávníček, K. Peszyński, J. Hošek and S. Wawrzyniak, Aerodynamic and mass transfer characteristics of an annular bistable impinging jet with a fluidic flip-flop control. *Int. J. Heat Mass Transfer* **46** 7 (2003), pp. 1265–1278.

17. S.C. Crow and F.H. Champagne, Orderly structure in jet turbulence. *J. Fluid Mech.* **48** (1971), pp. 547–591.

18. A.K.M.F. Hussain, Coherent structures—reality and myth. *Phys. Fluids* **26** 10 (1983), pp. 2816–2850.

19. K. Kataoka, M. Suguro, H. Degawa, K. Maruo and I. Mihata, The effect of surface renewal due to large scale eddies on jet impingement heat transfer. *Int. J. Heat Mass Transfer* **30** 3 (1987), pp. 559–567.

20. M. Gad-el-Hak, Modern developments in flow control. *Appl. Mech. Rev.* **49** (1996), pp. 365–379.

21. H.E. Fiedler and H.-H. Fernholz, On management and control of turbulent shear flows. *Prog. Aerospace Sci.* **27** (1990), pp. 305–387.

22. S.D. Hwang, C.H. Lee and H.H. Cho, Heat transfer and flow structures in axisymmetric impinging jet controlled by vortex pairing. *Int. J. Heat Fluid Flow* **22** 3 (2001), pp. 293–300.

23. C. Herman, The impact of flow oscillations on convective heat transfer. *Ann. Rev. Heat Transfer* **11** (2000), pp. 495–562.

24. S.D. Hwang and H.H. Cho, Effects of acoustic excitation positions on heat transfer and flow in axisymmetric impinging jet: main jet excitation and shear layer excitation. *Int. J. Heat Fluid Flow* **24** 2 (2003), pp. 199–209.

25. T.C. Corke and S.M. Kusek, Resonance in axisymmetric jets with controlled helical-mode input. *J. Fluid Mech.* **249** (1993), pp. 307–336.

26. J. Lepišovský, K.K. Ahuja and R.H. Burrin, Tone excited jets. Part III: Flow measurements. *J. Sound Vib.* **102** (1985), pp. 71–91.

27. J. Lepičovský, K.K. Ahuja and R.H. Salikuddin, An experimental study of tone-excited heated jets. *J. Propulsion Power* **2** 2 (1986), pp. 149–154.

28. E.V. Vlasov and A.S. Ginevskii, Acoustic modification of the aerodynamic characteristics of turbulent jet. *Mekhanika Zhidkosti i Gaza* **2** 4 (1967), pp. 133–138 (in Russian) .
E.V. Vlasov and A.S. Ginevskii, Acoustic modification of the aerodynamic characteristics of turbulent jet. *Fluid Dynamics* **2** 4 (1967), pp. 93–96.

29. E.V. Vlasov and A.S. Ginevskii, The aeroacoustic interaction problem (review). *Sov. Phys. Acoust.* **26** 1 (1980), pp. 1–7.

30. S.K. Cho, J.Y. Yoo and H. Choi, Vortex pairing in an axisymmetric jet using two-frequency acoustic forcing at low to moderate Strouhal numbers. *Exp. Fluids* **25** 4 (1998), pp. 305–315.

31. J. Vejražka, Experimental study of a pulsating round impinging jet, Ph.D. Thesis, Institut National Polytechnique de Grenoble, Grenoble 2002

32. C. Gau, W.Y. Sheu and C.H. Shen, Impingement cooling flow and heat transfer under acoustic excitations. *Trans. ASME J. Heat Transfer* **119** 4 (1997), pp. 810–817.

33. T. Liu and J.P. Sullivan, Heat transfer and flow structures in an excited circular impinging jet. *Int. J. Heat Mass Transfer* **39** 17 (1996), pp. 3695–3706.

34. H. Maki, A. Yabe, Unsteady characteristics of the annular impinging jet flow field and reverse stagnation point heat transfer, in: Proceedings of the National Heat Transfer Conference Heat Transfer in Convective Flows, HTD-Vol. 107, Philadelphia, PA, 1989, pp. 163–168

35. H. Maki and A. Yabe, Heat transfer by the annular impinging jet. *Exp. Heat Transfer* **2** (1989), pp. 1–12.

36. Y. Kokoshima, A. Shimizu, T. Murao, Numerical analysis of annular turbulent jet impinging on a flat plate, in: Proceedings of the 3rd Triennial Int. Symp. Fluid Control, Measurement, and Visualization, FLUCOME'91, ASME, San Francisco, USA, 1991, pp. 205–210

37. Z. Trávníček and F. Křížek, Impaktströmung und die Zusammengesetzte Schlitzdüse (Impinging jet and combined slot nozzle). *Heat Mass Transfer* **35** 5 (1999), pp. 351–356.

38. Z. Trávníček, F. Maršík, Flow visualization and mass transfer with a bistable two-slot impinging jet, in: Proceedings of the 10th Int. Symposium on Flow Visualization, (ISFV 10), Kyoto, 2002, Book of Abstracts p. 44; Full text CD-ROM, F0068

39. V. Tesař, M. Jílek and Z. Randa, Topology changes in an annular impinging jet flow. In: *Proceedings of the Topical Problems in Fluid Mechanics 2001*, Institute of Thermomechanics CAS, Prague (2001), pp. 121–124.

40. Z. Trávníček and V. Tesař, Annular synthetic jet used for impinging flow mass-transfer. *Int. J. Heat Mass Transfer* **46** 17 (2003), pp. 3291–3297.

41. B.L. Smith and A. Glezer, The formation and evolution of synthetic jets. *Phys. Fluids* **10** 9 (1998), pp. 2281–2297.

42. V. Tesař and S. Zhong, Efficiency of synthetic jets generation. *Trans. Aeronaut. Astronaut. Soc. Republic of China* **35** 1 (2003), pp. 45–53.

43. N.V. Ko and W.T. Chan, Similarity of the initial region of annual jets: three configurations. *J. Fluid Mech.* **84** 4 (1978), pp. 641–656.

44. F. Křížek, The wall mass transfer under annular jet impact flow. *Coating* **23** 3 (1990), pp. 74–77 (4) (1990) 128–132 .

45. R.J. Goldstein and H.H. Cho, A review of mass transfer measurements using naphthalene sublimation. *Exp. Therm. Fluid Sci.* **10** (1995), pp. 416–434.

46. M. Korger and F. Křížek, Mass-transfer coefficient in impingement flow slotted nozzles. *Int. J. Heat Mass Transfer* **9** 5 (1966), pp. 337–344.

47. S.J. Kline and F.A. McClintock, Describing uncertainties in single-sample experiments. *Mech. Eng.* **75** (1953), pp. 3–8.

48. W.T. Chan and N.V. Ko, Coherent structures in outer mixing region of annular jets. *J. Fluid Mech.* **89** (1978), pp. 515–533.

49. F.O. Thomas, Structure of mixing layers and jets. *Appl. Mech. Rev.* **44** (1991), pp. 119–153.